2-27-2020

Twentieth Century Black Carbon and Dust Deposition on South Cascade Glacier, Washington State, USA, as Reconstructed From a 158-m-Long Ice Core

Susan D. Kaspari
Central Washington University

Dan Pittenger
Central Washington University

T. M. Jenk
Paul Scherrer Institut

U. Morgenstern
National Isotope Centre, New Zealand

M. Schwikowski
Paul Scherrer Institut

See next page for additional authors

Recommended Citation

Kaspari, S. D., Pittenger, D., Jenk, T. M., Morgenstern, U., Schwikowski, M., Buenning, N., & Stott, L. (2020). Twentieth century black carbon and dust deposition on South Cascade Glacier, Washington State, USA, as reconstructed from a 158-m-long ice core. Journal of Geophysical Research: Atmospheres, 125, e2019JD031126. https://doi.org/10.1029/2019JD031126

JGR Atmospheres

RESEARCH ARTICLE
10.1029/2019JD031126

Key Points:
- An ice core from South Cascade Glacier, Washington (USA), is used to reconstruct black carbon and dust deposition spanning 1840–1991
- Peak black carbon deposition during 1940–1960 is 16 times higher than background black carbon levels
- Albedo reductions are dominated by dust, except during high BC deposition events from forest fires and the peak industrialization period

Supporting Information:
- Supporting Information S1
- Figure S1
- Figure S2
- Figure S3
- Figure S4
- Figure S5
- Figure S6

Correspondence to:
S. D. Kaspari,
kaspari@geology.cwu.edu

Citation:
Kaspari, S. D., Pittenger, D., Jenk, T. M., Morgenstern, U., Schwikowski, M., Buenning, N., & Stott, L. (2020). Twentieth century black carbon and dust deposition on South Cascade Glacier, Washington State, USA, as reconstructed from a 158-m-long ice core. *Journal of Geophysical Research: Atmospheres*, *125*, e2019JD031126. https://doi.org/10.1029/2019JD031126

Received 3 JUN 2019
Accepted 21 FEB 2020
Accepted article online 27 FEB 2020

Twentieth Century Black Carbon and Dust Deposition on South Cascade Glacier, Washington State, USA, as Reconstructed From a 158-m-Long Ice Core

S. D. Kaspari[1], D. Pittenger[1], T. M. Jenk[2,3], U. Morgenstern[4], M. Schwikowski[2,3,5], N. Buenning[6], and L. Stott[6]

[1]Department of Geological Sciences, Central Washington University, Ellensburg, WA, USA, [2]Laboratory of Environmental Chemistry, Paul Scherrer Institut, Villigen, Switzerland, [3]Oeschger Centre for Climate Change Research, University of Bern, Bern, Switzerland, [4]Institute of Geological and Nuclear Sciences, National Isotope Centre, Lower Hutt, New Zealand, [5]Department of Chemistry and Biochemistry, University of Bern, Bern, Switzerland, [6]Department of Earth Sciences, University of Southern California, Los Angeles, CA, USA

Abstract Light absorbing particles (LAPs) include black carbon (BC) and mineral dust and are of interest due to their positive radiative forcing and contribution to albedo reductions and snow and glacier melt. This study documents historic BC and dust deposition as well as their effect on albedo on South Cascade Glacier (SCG) in Washington State (USA) through the analysis of a 158-m (139.5-m water equivalent [w.e.]) ice core extracted in 1994 and spanning the period 1840–1991. Peak BC deposition occurred between 1940 and 1960, when median BC concentrations were 16 times higher than background, likely dominated by domestic coal and forest fire emissions. Post 1960 BC concentrations decrease, followed by an increase from 1977 to 1991 due to melt consolidation and higher emissions. Differences between the SCG record and BC emission inventories, as well as ice core records from other regions, highlight regional differences in the timing of anthropogenic and biomass BC emissions. Dust deposition on SCG is dominated by local sources and is variable throughout the record. Albedo reductions from LAP are dominated by dust deposition, except during high BC deposition events from forest fires and during 1940–1960 when BC and dust similarly contribute to albedo reductions. This study furthers understanding of the factors contributing to historical snowmelt and glacier retreat in the Cascades and demonstrates that ice cores retrieved from temperate glaciers have the potential to provide valuable records of LAP deposition.

Plain Language Summary Light absorbing particles (LAPs) include black carbon (BC, i.e., soot) produced by the incomplete combustion of fossil and biofuels and mineral dust. In the atmosphere, LAP can lead to atmospheric warming, while LAP deposited on snow and glaciers causes darkening, leading to increased solar energy absorption, warming, and faster melt. The role of LAP in climate change is a large source of uncertainty because LAP emissions and deposition are spatially and temporally heterogeneous. We used an ice core retrieved from South Cascade Glacier in Washington State (USA) to reconstruct BC and dust deposition. BC deposition between 1940–1960 is 16 times higher than during the preindustrial period, likely dominated by domestic coal and forest fire emissions. Differences between the SCG ice core and BC emission inventories, as well as ice cores from other regions, highlight regional differences in BC emissions from humans and forest fires. Dust is a larger contributor to snow darkening than BC, except during high BC deposition events from forest fires and during the 1940–1960 period when BC and dust contribute comparably. This study furthers understanding of the role of BC and dust in snow and glacier melt in the Washington Cascades.

1. Introduction

Light absorbing particles (LAPs) contribute to climate change due to their positive radiative forcing (Bond et al., 2013; Flanner et al., 2007; Miller & Tegen, 1998). In the atmosphere, LAPs absorb energy and lead to atmospheric heating (Moosmuller et al., 2009), whereas LAPs deposited on snow and ice surfaces lead

to darkening, resulting in lower albedo and accelerated snow and glacier melt (e.g., Kaspari et al., 2015; S. M. Skiles et al., 2018; Warren, 1984). In some mountain environments, LAPs are a larger driver of snowmelt than atmospheric temperature (S. M. Skiles et al., 2012). LAPs include black carbon (BC) and dust, both of which can have natural and anthropogenic sources. BC is produced by the incomplete combustion of fossil and biofuels and is estimated to be second only to CO_2 in its contribution to recent climate warming (IPCC, 2013). Natural dust sources include arid regions and rocky outcrops; however, dust production has increased in some regions due to anthropogenic activities including land use change in the form of clearing and development and agricultural and grazing practices that reduce vegetation cover and break up the soil matrix (J. C. Neff et al., 2008; Tegen et al., 2004). BC and dust both have short atmospheric residence times, leading to regionally heterogeneous deposition. Thus, LAPs remain a large source of uncertainty in analyses of climate change because of their spatial and temporal variability (Bond et al., 2013; IPCC, 2013; Ramanathan & Carmichael, 2008).

Historical BC emissions have been estimated based on fossil and biofuel inventories, but these inventories have large sources of uncertainty and do not do well at capturing regional variability (Bond et al., 2007; Ito & Penner, 2005; Mieville et al., 2010; Mouillot & Field, 2005; Novakov et al., 2003). Thus, observational records that capture spatial and temporal variations in LAP are needed. In recent years, ice cores from mountain glaciers and ice sheets have been used to reconstruct BC depositional histories globally, including the Arctic with records from Greenland (e.g., McConnell et al., 2007) and Svalbard (Osmont et al., 2018); the European Alps (e.g., Sigl et al., 2018); the Caucasus (Lim et al., 2017); Asia (e.g., Kaspari et al., 2011; Ming et al., 2008; M. Wang et al., 2015); South America (Osmont et al., 2019); and Antarctica (e.g., Bisiaux et al., 2012). These records indicate a high level of regional variability in BC deposition associated with differences in the timing and scale of industrialization (discussed in section 3.5).

Two records of LAP deposition from ice cores extracted in Canada provide the only historical observational records of BC deposition in North America outside of the Arctic. A BC record from southwest British Columbia spanning 1973–2010 (P. Neff et al., 2012) record showed a clear seasonal signal, but the relatively short length of the record precludes information on historical trends during industrialization in the region. An ice core from Mt. Logan in the Yukon Territory, Canada, spanning 1852–1999 showed a constant BC background deposition rate with periodic BC peaks linked to regional forest fire activity in Alaska and Siberia but no strong temporal trends (Menking, 2013).

Reconstructing LAP depositional histories in the Cascade Range in Washington State is of interest because Washington has the highest concentration of glaciers in the contiguous United States and melt water from these glaciers provides an important source of water resources (Riedel & Larrabee, 2011). As in most alpine regions, glaciers in Washington are retreating (Riedel & Larrabee, 2011). While warming temperatures and decreased snow accumulation are well-recognized factors leading to glacier retreat in this region (McCabe & Fountain, 2013; Rasmussen et al., 2000), the deposition of LAP also contributes to accelerated melt. A shallow ice core retrieved from Snow Dome on Mt. Olympus in Washington State had high LAP concentrations (BC = 3,120 μg/L; gravimetric particles = 1,870 mg/L) that were linked to forest fire activity and accelerated snowmelt (Kaspari et al., 2015).

Here we present a historical record of LAP deposition spanning 1840–1991 reconstructed from the South Cascade Glacier (SCG) ice core from the North Cascades in Washington State, USA. The ice core has been analyzed for refractory BC (rBC) and gravimetric particles as a proxy for dust to document how LAP deposition has changed over the past century and how past depositional events have lowered snow and glacier albedo. Herein, rBC is used to refer to BC concentrations determined by laser-based incandescence, while the general term BC is used to refer to qualitative discussions of BC (Petzold et al., 2013). Understanding the depositional history of LAP on SCG will provide insight into the role of LAP in climate change in Washington State, including atmospheric radiative forcing, as well as snowmelt and glacier retreat.

2. Materials and Methods

2.1. Study Site

SCG (48°21′23.00″N, 121°3′26.65″W) is a temperate glacier located in the Cascade Mountains of north central Washington State (Figure S1 in the supporting information). The climate is maritime, characterized by

mild and dry summers and cool winters with high winter precipitation. The SCG is a benchmark glacier monitored by the United States Geological Survey (USGS) since 1953 (Anslow et al., 2008). SCG is retreating and has undergone a cumulative net loss of 67% of its estimated 1,890 volume as of 2007 (Josberger et al., 2017). The highest elevation of SCG is ~2,130 m, which is lower than sites typically selected for ice core retrieval for this latitude range. Because LAP can remain preserved under temperate conditions (Xu et al., 2012), this site provides the opportunity to reconstruct LAP deposition in a region of the world with no historical LAP records prior to the 1970s.

2.2. Ice Core and Snow Sample Retrieval and Processing

In 1994, USGS scientists and Polar Ice Coring Office (PICO) drillers extracted a 158-m-long (139.5-m water equivalent [w.e.] based on ice core density measurements) ice core from the accumulation zone (2,030 m a.s.l.) of SCG using a 9-cm thermal drill and reported that the ice core reached bedrock. After extraction, the ice core was shipped frozen and stored at the National Ice Core Laboratory in Denver, CO. In 2013, a one-quarter cross section of the ice core was processed at the National Ice Core Laboratory for rBC, water isotope, and gravimetric particle analyses. The one-quarter cross section of the ice core was cut into three longitudinal sections, with one inner section and two outer sections. The inner section was sampled into 1,983 samples (2.5 × 2.5 × ~7.75 cm; length varied from 4 to 10 cm) for rBC analysis, and the samples were stored in polyethylene bags (WhirlPak). One of the outer core sections was sampled at the same depth resolution as BC, with 196 samples (three to nine samples collected every 7 m) allocated for ^{210}Pb analysis, and the remaining 1,787 samples allocated for stable isotope analysis (δD and δ^{18}O). The other outer core section was processed into 198 sections (length varied between 15–132 cm) for gravimetric particle analysis. Details on tritium sampling are provided in section 2.3.6. All samples were shipped frozen to the institutions where they were analyzed (described further below).

In October 2014, additional snow samples were taken from the surface of SCG to determine the organic content of particles and mass size distribution of mineral dust deposited on SCG (described further in sections 2.3.3 and 2.3.4 below). The samples were shipped frozen to Central Washington University (CWU).

2.3. Sample Analysis

rBC, gravimetric particles, particle size distributions, and thermogravimetric analyses were conducted to develop the SCG BC and dust records, while stable isotopes, tritium, ^{210}Pb, and identification of the Mt. St. Helens ash layer were conducted to develop the SCG ice core depth age scale.

2.3.1. Refractory BC

The samples for rBC analyses were further processed at CWU. The outer section of the samples was decontaminated to remove potential external contaminants. The upper 23 m of the core was hand scraped using a ceramic scalpel, and the remainder of the core was rinsed with ultrapure water (~18 MΩ cm) and placed into acid-cleaned polypropylene vials. The ice samples for rBC analysis were transferred into the vials and stored frozen until ready to be analyzed.

Just prior to analysis, the rBC samples were melted, and the liquid samples were sonicated for 20 min. Immediately after sonication, the samples were placed on a magnetic stir plate where they were agitated using a magnetic stir bar. The melted, agitated sample was transferred with a peristaltic pump (Ismatec Reglo) into an ultrasonic nebulizer (Cetac U5000+), from which the dry aerosols were introduced to the sample inlet of the Single Particle Soot Photometer (SP2, Droplet Measurement Technologies) for rBC analysis. The SP2 uses laser-induced incandescence to determine the size and abundance of rBC on a per-particle basis (Schwarz et al., 2006), which can then be used to calculate the rBC liquid mass concentration. Further details on the analytical method are presented in Kaspari et al. (2014), Kaspari et al. (2015), and Wendl et al. (2014).

2.3.2. Gravimetric Particles

Processing of the ice core sections for gravimetric particle analysis was also conducted at CWU. The upper 23 m of the core was hand scraped using a ceramic scalpel, and the remainder of the samples were rinsed with ultrapure water and stored frozen in Pyrex jars until analysis. Samples were melted, sonicated, and filtered through preweighed 0.45-μm pore size, mixed cellulose ester membrane filters (Millipore HAWP02400) using a vacuum pump, and dried in a laminar flow box. The filters were weighed with a microbalance with a precision of 0.003 mg. Particle concentration was determined using the mass of the

filtered particles and the mass of the ice (Kaspari et al., 2015). Because of the coarser resolution of the gravimetric method, several years of deposition might be covered by one sample.

2.3.3. Particle Size Distribution

Determining the particle size distribution of mineral dust is necessary to quantify the albedo reduction resulting from dust deposition (Flanner et al., 2007; Flanner et al., 2009). Bulk snow samples were collected from the top centimeter of SCG in October 2014 and transported frozen to CWU where they were used to determine the particle size distribution of mineral dust. The bulk snow samples were melted at room temperature in preweighed, clean Pyrex jars and refrigerated until ready to analyze. Prior to analysis, the water was evaporated in a drying oven at 60 °C, and the remaining particles were transferred into preweighed ceramic crucibles for loss on ignition, which was used to remove the organic fraction of the sample. The sample was heated at 400 °C for 4 hr, and the remaining sediment in the crucible was then considered to be the mineral dust component of the sample.

The mass size distribution was determined in small subsamples (~400 mg) of the mineral dust sample with a laser diffractometer (Malvern Mastersizer 2000) using the methodology established by Sperazza et al. (2004) specifically for fine-grain sediments. Three samples were measured, with six mass size readings taken per sample. The 18 particle size distributions were then averaged to determine the particle size distribution.

2.3.4. Thermogravimetric Analysis to Determine Organic Content

The organic content of the particles was determined in six bulk snow samples that were collected from the surface of SCG in October 2014, which in turn allowed the mineral dust component of the gravimetric particulates to be deduced. Thermogravimetric analysis was conducted at the Paul Scherrer Institut using a NETZSCH STA 449C analyzer equipped with a ThermoStar Pfeiffer Vacuum mass spectrometer. All the measurements were performed in flowing (30 ml/min) helium containing 20 vol.% of oxygen. The samples were heated up to 800 °C at a rate of 5 °C/min, annealed at 800 °C for 60 min, and finally cooled at a rate of 20 °C/min. A change of the mass observed within temperature range 150–800 °C was assumed to be directly related to the content of organic components in the samples as all organic material should be completely oxidized creating volatile gas products.

2.3.5. Stable Isotopes

Stable isotope ($\delta^{18}O$ and δD) analysis was conducted at the University of Southern California. Each sample was melted in a WhirlPak bag that was enclosed in an additional plastic airtight bag to avoid fractionation (during evaporation) and equilibration with ambient air. Each plastic container was subjected to room temperatures, allowing the ice samples to slowly melt (between 30 and 90 min). Once the ice was completely melted within the plastic containers, the water was immediately transferred to autosampler vials to determine $\delta^{18}O$ and δD with a cavity ring down spectrometer (Picarro L1102i). The raw isotope results were calibrated to VSMOW using a simple linear equation based on a least-squares fit to international standards that were measured with the same instrument. Every eighth sample was an in-house water sample of known isotopic composition to monitor precision and accuracy. The standard deviation of the in-house standards analyzed during the study was 0.08‰ for $\delta^{18}O$ and 0.67‰ for δD.

2.3.6. Tritium

Tritium (^{3}H) was analyzed at the National Isotope Center in New Zealand, to identify the 1963 tritium peak associated with atmospheric hydrogen bomb testing (Morgenstern & Taylor, 2009). To isolate the tritium peak, a first set of samples was analyzed at roughly 10-m w.e. resolution. The results indicated that the tritium peak likely resided between 20- and 0-m w.e.; thus, an additional set of samples taken at 1-m resolution between 20- and 40-m w.e. was sent for further analyses. Finally, samples between 28- and 30-m w.e. were analyzed at high resolution.

Tritium β-activity was determined by low-level liquid scintillation counting (Quantulus) according to Morgenstern and Taylor (2009) without prior tritium enrichment. In 20-ml PE vials, 8 ml of sample water was mixed with 12 ml of scintillation cocktail (Quicksafe 400) and measured for 2,000 min to achieve a detection limit of 3 TU.

2.3.7. ^{210}Pb

A product of the natural ^{238}U decay series, ^{210}Pb, is a natural radionuclide, which is attached to aerosol particles in the atmosphere and eventually deposited in the environment, for example, on glaciers with fresh snow. It has a half-life of 22.3 years resulting in an accessible dating range of about 100–150 years, and allows the depth age scale of ice cores to be constrained (Eichler et al., 2000; Gabrielli et al., 2016; Gäggeler et al.,

1983; Olivier et al., 2006; C. Wang et al., 2014). More recently, this method was also applied successfully to constrain the dating of an ice core from a temperate glacier (Pavlova et al., 2015). The SCG ice core was sampled for ^{210}Pb at ~5-m discontinuous intervals and processed for final measurement by α-spectroscopy at the Paul Scherrer Institute following the standard method established by Gäggeler et al. (1983).

2.3.8. Microscopic Identification of 1980 Mt. St. Helens Ash Layer

Ash deposition from the 7 August 1980 Mt. St. Helens eruption was observed on SCG (B. Jacobel, personal communication, December 2017), consistent with north-northeast transport of ash reported for this eruption (Waitt & Dzurisin, 1981). The gravimetric particle filters were examined for ash. The gravimetric filter corresponding to 1980 had high particulate loading (141,900 ng/g), and microscopic examination of the filter indicated the presence of plagioclase, amphiboles, and hornblende consistent with Mt. St. Helens ash (J. Blundy, personal communication, May 2018), thus providing a reference horizon for the ice core depth age scale.

2.4. Ice Core Depth Age Scale

The upper 40-m w.e. of the SCG depth age scale was established using a combination of ages obtained from reference horizons (tritium from nuclear fallout in 1963 (Morgenstern & Taylor, 2009) and ash layer from the 1980 eruption of Mt. St. Helens), glacial mass balance records (McNeil et al., 2016), and annual layer counting, while below 40-m w.e., the ice core was dated using ^{210}Pb dating (Gäggeler et al., 1983) and a glacier flow model (Dansgaard & Johnsen, 1969) (Figure 1). The most certain dating horizons in the ice core chronology are from the high-resolution 1963 tritium peak located at 27.5-m w.e. and identification of Mt. St. Helens ash at 8.9-m w.e.

2.4.1. Mass Balance Record

The ice core depth age scale was constrained by annual mass balance data spanning 1953–1994 provided by the USGS (McNeil et al., 2016). Glacier mass balance is calculated based on 5–10 winter accumulation and summer ablation points located in a transect parallel with glacial flow and marked with aluminum poles anchored in the glacial ice. The SCG ice core was drilled near the head of the glacier at an elevation of 2,030 m and within 200 m of mass balance Site 2030. Mass balance data from Site 2030 were available between 1986 and 2011. In order to constrain mass balance at the drill site prior to 1986, the difference between whole glacier mass balance and mass balance at Site 2030 was calculated resulting in a value of 1.16 ± 0.51-m w.e. (Table S1; the two data sets are significantly correlated: $n = 24$; $r^2 = .81$; $p < 0.01$). The resulting value, 1.16 ± 0.51-m w.e., was then applied to whole glacier mass balance data back to the beginning of initial collection in 1953, where 1.16 ± 0.51-m w.e. additional annual accumulation occurred at Site 2030 when compared to the glacier-wide mass balance. The 1963 tritium horizon was used to further constrain accumulation at the drill site, yielding an average annual accumulation of 1.45-m w.e. greater than the glacier-wide mass balance and within the 1σ uncertainty. The 1.45-m w.e. was then added to each year's glacier-wide mass balance measurement, resulting in a recorded depth of 40-m w.e. at 1953 (Figure 1). Based on the mass balance data, years with negative balance result in the years 1979, 1988, 1989, and 1992–1994 missing from the SCG record.

2.4.2. Annual Layer Counting

In the SCG region, peak deposition of trace elements, rBC, and dust occurs during the summer when dry conditions are present (Kaspari et al., 2015), and precipitation records indicate that stable isotopes (δ^{18}O and δD) are least negative during summer (Buenning et al., 2012). Because SCG is temperate, melt water percolation resulted in a diffuse stable isotope signal; the amplitude of the δ^{18}O in SCG was usually 2‰, compared to ~8–10‰ in the Mount Waddington ice core record in British Columbia (P. Neff et al., 2012). The Mt. St. Helens and tritium horizons and mass balance data were the primary SCG dating tools, with the rBC and stable isotope records used in conjunction with the mass balance data to identify the location in the core of the annual layer horizons (Figure S3). Combining these methods, annual layers were identified to a depth of 40-m w.e., where the date was determined to be 1954 ± 5 years.

2.4.3. Glacier Flow Modeling

The Dansgaard-Johnsen glacier flow model accounts for glacial thinning with depth and was investigated to further constrain the SCG ice core depth age scale (Dansgaard & Johnsen, 1969). This model approximates the horizontal velocity profile described by Glen's law for a plastic solid such as ice, assuming a constant horizontal velocity equal to the surface velocity u_s down to a distance h above the bed (i.e., the thickness of the bottom shear layer). Below h, the horizontal velocity decreases linearly until reaching 0 at bedrock or, in case

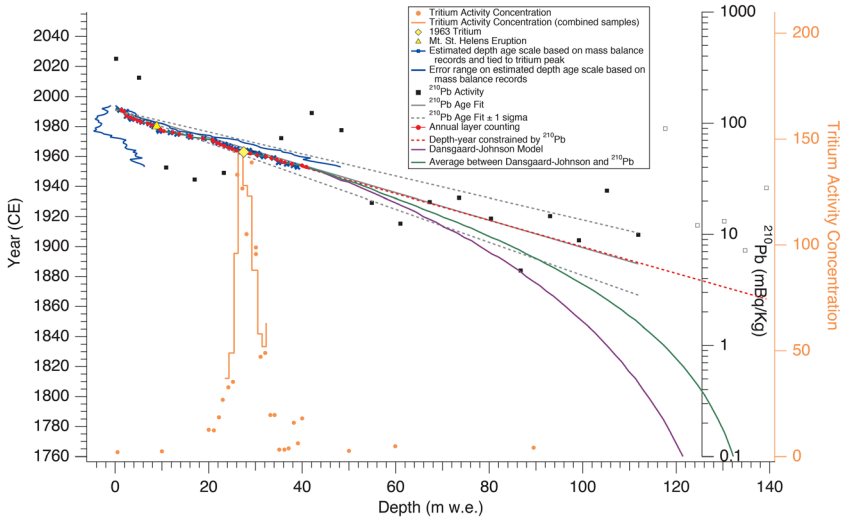

Figure 1. The South Cascade Glacier ice core depth age scale. Orange dots show tritium activity from individual samples, whereas the orange line shows tritium activity for continuous sections of core where samples were combined. The yellow diamond indicates the 1963 tritium horizon, and the yellow triangle indicates the 1980 horizon from the Mt. St. Helens volcanic eruption. The blue lines indicate the upper and lower depth age based on the glacier mass balance records (Table S1), and the blue line with crosses indicates the estimated depth age based on mass balance records constrained by the 1963 tritium horizon. The red dots indicate the BC and isotope annual layer counting, which is constrained by the Mt. St. Helens and tritium horizons, and the glacier mass balance records. Solid black squares indicate ^{210}Pb concentration after background correction, and the open black squares indicate samples in which the dust likely did not originate from aeolian deposition and thus were excluded from dating. The gray solid and dashed lines indicate the ^{210}Pb best fit age and the ^{210}Pb $\pm$ 1σ, respectively. The red dashed line is the depth age scale below the annual layer counting, as constrained by ^{210}Pb (youngest dating scenario). The purple line is the depth age scale based on the Dansgaard-Johnsen model (oldest dating scenario). The green line is the highest probability estimate, based on the average between the Dansgaard-Johnsen model (purple line) and ^{210}Pb best fit (red dashed line).

of basal sliding, the sliding velocity at the bed, u_b. The model, which assumes steady-state conditions, can be solved yielding an age t for any given depth y if, besides u_s, u_b, and h, the ice thickness H and the average annual accumulation rate b are known. However, this is usually not the case. One possible solution is to find a best fit of the model to the observational data (e.g., distinct time horizons found in the ice core and annual layer-counted ages at given depths) by tuning a subset of parameters such as h and b while using a best estimate or rely on glaciological measurement data for the others (e.g., H from ground-penetrating radar or surface flow velocities from stake measurements). In the case of SCG, certainty in dating accuracy only exists for the time horizons above 27.5-m w.e. depth (uppermost 20% of the core) where only slight thinning is assumed. Hence, a fit to the observational data is not feasible for SCG or at least would not strongly constrain the model. Thus, we use reasonable, best estimates for all parameters. Glacier thickness H was 145-m w.e., which is slightly larger than the 139.5-m w.e. measured in 1994, thereby accounting for the negative mass balance years observed in the more recent past (see Table S1). Accumulation b was set to 1.2-m w.e./a, and the bottom shear zone thickness h was set to 14.5-m w.e. (10% of H), which we assumed to be a reasonable value for a temperate glacier. Surface flow velocity u_s is 5 m/a, based on measurements for the core site. The sliding velocity at the bed u_b was estimated to be 0.5 m/a (i.e., 10% of u_s; A. Fountain, personal communication, November 2019), which is consistent with the value used in Neff et al. (2012). Lastly, we assumed a basal melt rate of 0.05 m/a, similar to the value modeled for the upper 0–25 km of the accumulation zone of Columbia Glacier in Alaska, USA (Alexander et al., 2013).

2.4.4. ^{210}Pb Record

The ^{210}Pb activity signal in SCG shows high variability and scatters around the expected exponential decrease with depth (radioactive decay with time). Even in the deepest part of the record, typical ^{210}Pb background levels of around 2–5 mBq/kg from supported ^{210}Pb (in situ produced ^{210}Pb from the decay of ^{238}U, which is part of the ice-contained mineral dust) are not reached.

A possible reason for the observed variability is displacement of ^{210}Pb with percolating melt water or enrichment in layers when years with negative glacier mass balance at the site occur resulting in accumulated multiyear deposition in the same layer (see section 3.4). Such effects are obviously of high relevance for ice cores extracted from sites close to the equilibrium line, particularly in the case of temperate glacier conditions. Nevertheless, it has been shown that ^{210}Pb records even from such sites still allow for dating, although associated with an increase in uncertainty (Pavlova et al., 2015).

The absence of typical background levels is usually an indication for the age of the samples being younger than four to five half-life times of ^{210}Pb (implying that near complete decay has not yet been reached). However, in the presence of high dust content, background levels can be unexpectedly high (e.g., >10 mBq/kg, Hou et al., 2018) and in this case may not be recognized as such. Here, very high dust concentrations were found in the lowermost part of the core, likely not related to aeolian deposition (see section 3.6; Figure S2). Samples from this section were accordingly excluded for the ^{210}Pb dating, and a value of 6.5 mBq/kg, the lowest activity observed in the core minus 3σ, was used for the background subtraction. Under these arguably reasonable assumptions, the dating by ^{210}Pb for the depth of the 1963 tritium horizon (27.5-m w.e) results in very good agreement with 1966 $\pm$ 5 (1σ). This shows that ^{210}Pb in the SCG core can provide a reasonable and independent age constraint at least down to a depth of 128 m (112-m w.e.).

2.4.5. Depth Age Scale Summary

The final depth age scale of the ice core was constrained using the 1963 tritium and 1980 Mt. St. Helens ash horizons, glacier mass balance records, and annual layer counting (Figure 1). Based on these methods, the age at 40-m w.e. of the core was determined to be 1954 $\pm$ 5 years. Because our confidence in dating accuracy is very high down to 27.5-m w.e. (1963) but due to the lack of precise constraint substantially decreases thereafter, we present three dating scenarios that bracket the potential depth age range of the SCG core below 40-m w.e.: (1) the youngest dating scenario, where the ice core dating is constrained by the ^{210}Pb data and in which no thinning with depth is assumed, (2) the oldest dating scenario based on the Dansgaard-Johnsen model (1969) with model parameters as described in section 2.4.3, and (3) the highest probability dating scenario, which is the average between the youngest and oldest dating scenarios, which define the lower and upper age estimate (i.e., dating uncertainty), respectively (Figure S4). In section 3, all three dating scenarios are presented. Herein, we present results to a depth of 115-m w.e., where the three dating scenarios yield an age between 1886 CE (based on the ^{210}Pb dating) and 1795 CE (based on the Dansgaard-Johnsen model), with the average age being 1840 CE. We do not interpret the record below 115-m w.e. due to high dust loading, which likely does not originate from aeolian deposition (Figure S2; section 3.6). Further, the high dust loads can result in a positive rBC artifact during sample analysis (Schwarz et al., 2012).

2.5. Modeled Albedo Reductions

With the dust and rBC data, historic albedo reductions were calculated using the Snow, Ice, and Aerosol Radiation (SNICAR) model (Flanner et al., 2007). The SNICAR model allows for set user-defined environmental variables to remain constant while concentrations of rBC and dust are adjusted to match observed concentrations. SNICAR has been shown to be an effective means of modeling snow albedo based on laboratory (Hadley & Kirchstetter, 2012) and field studies (e.g., Kaspari et al., 2015).

SNICAR model inputs for the SCG ice core are as follows: Incident solar radiation was set as diffuse midlatitude sky conditions, representing cloudy or hazy skies. Snow grain size retrieved using a spectroradiometer following the methods of Painter et al. (2007) on SCG in October 2014 varied from 400 to 700 μm at the peak of summer melt consolidation. For the results reported herein, we used a grain size of 500 μm. Snowpack thickness was set as 158.3 m based on the length of the ice core. Setting the snowpack thickness to a thickness representative of the seasonal snowpack had a negligible effect on the results. The dust size distribution was constrained by dust collected from the surface of SCG in October 2014 and measured in the Mastersizer and entered using a lognormal function with a median particle diameter of 14.05 μm and a 1σ of 2.89 μm. The optical properties of the dust were based on the central hematite scenario (by volume 1.5% hematite, 31.5% illite, 14% quartz, 6% calcite, 24% kaolinite, 23% montmorillonite) defined by Balkanski et al. (2007). BC was entered as uncoated particles with a mass absorption cross section of 7.5 m^2/g at 550 nm based on Bond and Bergstrom (2006).

2.6. Historical BC Emission Data

BC emission data were acquired from the Representative Concentration Pathways database (Version 2.0; https://tntcat.iiase.ac.at/RcpDb), which provides gridded historical emission data of forest fires (Mieville et al., 2010; Mouillot & Field, 2005; Schultz et al., 2008) and energy-related combustion from fossil and biofuels (Bond et al., 2007). Emission data were acquired from the grid cell where SCG is located (northwest coordinates = 49.0,−122.0; southeast coordinates = 48.0,−121.0; referred to as "local") and from a larger region (northwest coordinates = 50.0,−124.0; southeast = 47.0,−121.0; referred to as "regional") that encompasses large population centers (e.g., Seattle, WA, and Vancouver, BC) that emit BC that may be transported to SCG. Because BC may originate from regions further away, we also compare the SCG rBC record to the energy-related BC emission inventories from the United States and East Asia as provided by Bond et al. (2007). Based on proximity to sources and dominant atmosphere circulation pathways, BC emissions from these larger regions may also contribute to BC deposited at SCG (Bond et al., 2007; Hadley et al., 2007; Hu et al., 2019).

3. Results and Discussion

3.1. Historical BC Record

The SCG ice core rBC record indicates that BC deposition in this region has been temporally variable (Figure 2, Table 1). Here we interpret both changes in the long-term trend (represented by the smoothed line in Figure 2b) and intermittent high concentration horizons. The period between 1840–1890 is interpreted to represent background BC concentrations for this region. Post 1890 rBC concentrations begin to increase, with peak rBC concentrations occurring between 1940–1960. Both background and maximum rBC concentrations increase during this period, with median rBC concentrations between 1940–1960 ~16-fold higher than background levels, likely reflecting peak industrialization in the region (section 3.2). Post 1960 rBC concentrations decrease, which may reflect the phase in of air pollution regulations (e.g., 1963 Clean Air Act) and a transition away from coal and wood heating. From ~1977 to the most recent part of the record, rBC concentrations increase, likely tied to an increase in atmospheric BC emissions and melt consolidation (discussed further in sections 3.2 and 3.4, respectively).

3.2. Comparison of the SCG Ice Core rBC Record With Historical BC Emission Inventories

A comparison of the SCG rBC record with historical BC emission inventory data (section 2.6) shows the strongest similarities with regional emissions, particularly domestic emissions during the 1940s–1960s (Figure 2d). Emission inventories for the local, regional, and the United States (Figures 2c, 2d, and 2f) all indicate that BC emissions increased steadily to peak emissions during the 1920s associated with domestic coal use; a reduction during the 1930's depression; and a subsequent increase during the 1940s (the United States) or 1950s (local and regional) (Bond et al., 2007).

While peak rBC concentrations in the SCG ice core record are coincident with the regional domestic BC emissions during the 1950s, the SCG record does not reflect the earlier peak in BC emissions during the 1920s. This may be due to the emission inventories not capturing the timing and magnitude of regional anthropogenic emissions. Population growth (Figure 2g) and industrial development occurred later in the Pacific Northwest than the United States as a whole due to lack of railroad transportation. The completion of three transcontinental railroads (northern Pacific railroad in 1883; the Great Northern railroad in 1893; and the Canadian Pacific railroad in 1885) opened up the west to population growth and industrialization. Coal mining took place at many sites in the region by the late 1800s, and coal was used to fuel locomotives and steamships and for domestic heating (McCarty, 2003; Schwantes, 1996). The timing of the opening of the railroads and coal mining, and slow rise in population, is consistent with the rise in SCG rBC above preindustrial levels that begins in the late 1800s. Population growth increases in Washington post–World War II, consistent with the peak rBC concentrations from 1940–1960. During the 20th century, oil, hydroelectricity, and natural gas became important energy sources; however, coal and wood burning, both sources of BC emissions, remained an important source of energy for home heating into the 1960s. The peak in SCG rBC during the 1940–1960 period likely reflects large-scale wood and coal heating by the growing population; post 1960, the region transitioned to oil and natural gas. Additionally, the SCG rBC record includes forest fire emissions that can be a major source of BC in this region (discussed in section 3.3), which are not captured by the energy-related emission inventories (Bond et al., 2013).

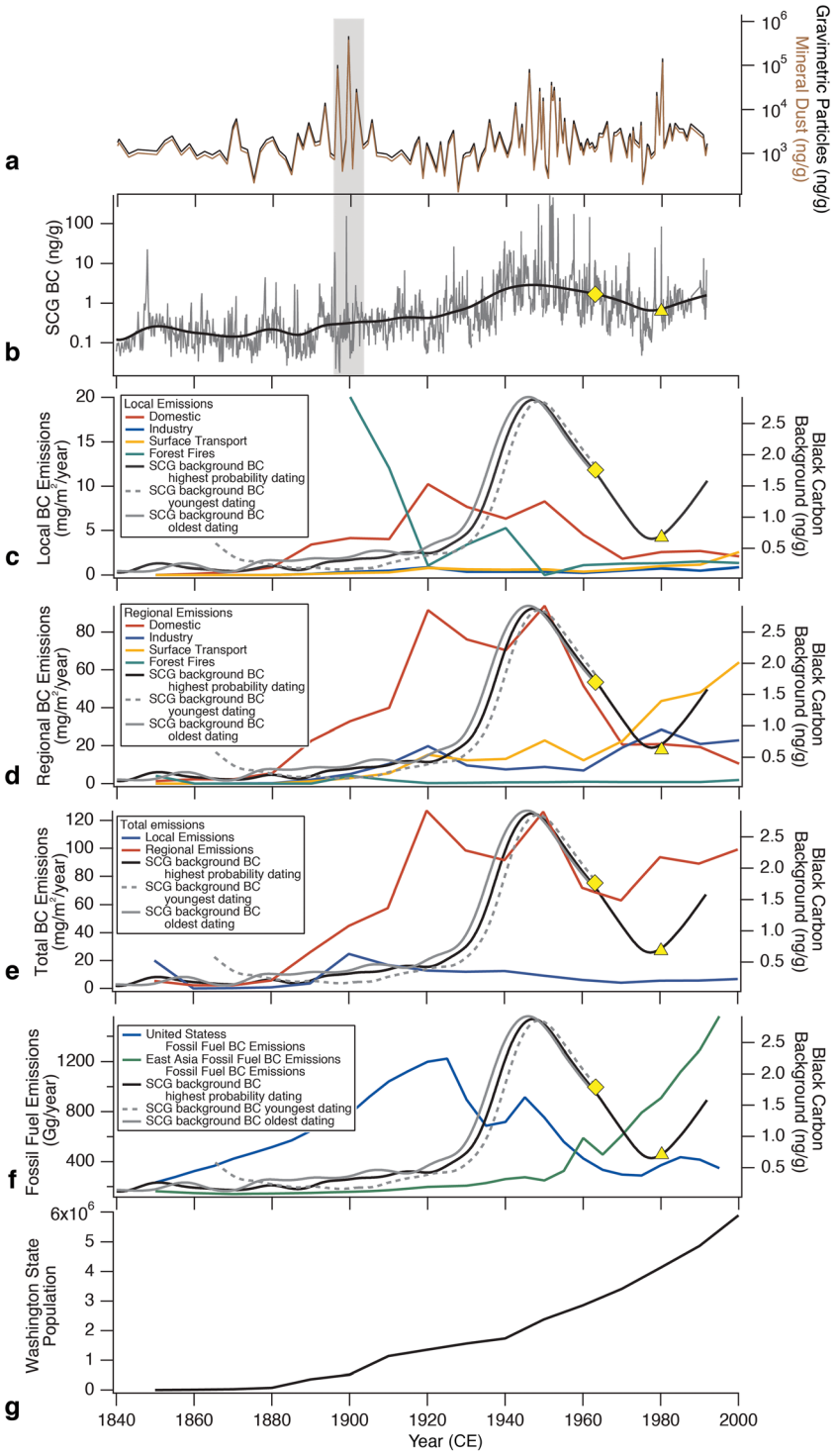

Figure 2. (a) South Cascade Glacier (SCG) gravimetric particle (black) and estimated mineral dust component (brown), (b) high-resolution SCG black carbon (rBC) record (gray) and robust spline-smoothed rBC record (black), (c) local anthropogenic and forest fire BC emissions, (d) regional anthropogenic and forest fire BC emissions, (e) local and regional total BC emissions (anthropogenic + forest fire), (f) BC energy-related emission inventory data for the United States (red line) and East Asia (blue line) (Bond et al., 2007), and (g) Washington State population (United States Census Bureau). (c)–(f) include the robust spline-smoothed rBC record based on the youngest (gray dashed line) highest probability (black line) and oldest (solid gray line) dating scenarios. The areas covered by the local and regional emissions are defined in section 2.6. The yellow triangle and yellow diamond identify the 1980 Mt. St. Helens and 1963 tritium horizons, respectively. The gray highlighted rectangle in (a) and (b) identifies the portion of the record that has high melt, and the LAP layers may be caused by englacial flow rather than aeolian deposition.

Table 1
South Cascade Glacier Black Carbon Median, Mean, and Maximum Concentrations for the Periods Indicated (Based on the Highest Probability Dating Scenario) and Median Increase Factors Relative to Background Concentrations

Period	1840–1890	1940–1960	1977–1991
Median rBC (ng/g)	0.1	2.2	0.9
Mean rBC (ng/g)	0.3	11.8	1.9
Maximum rBC (ng/g)	22.8	524.6	84.7
Median increase factor relative to background		16.0	6.2
Interpretation	Background BC	Peak industrial BC deposition	Melt consolidation and/or increased BC deposition

The post 1980's increase in the SCG rBC record is coincident with an increase in BC emissions from surface transportation (Figures 2d and 2e), as well as rising East Asian emissions. Thus, the rising rBC concentrations in the uppermost portion of the core could be due to increased deposition from regional or long-range sources. BC emitted in East Asia can undergo trans-Pacific transport from East Asia to the western United States, particularly during spring (Hadley et al., 2007; Hu et al., 2019; Jaffe et al., 1999). East Asian BC emissions begin a steady rise in the mid-20th century and are a substantial source of global BC emissions by the late 20th century (Bond et al., 2007; Novakov et al., 2003; Figure 2f). While trans-Pacific transport of BC emissions from East Asia may contribute to the rise in rBC observed in the SCG ice core post 1980, the contribution is likely minor. This is supported by BC seasonality; trans-Pacific aerosol transport is highest during spring, while BC concentrations in the SCG region are highest during summer (Delaney et al., 2015). Rather, the post 1980's increase in SCG rBC is likely dominated by melt consolidation and to a lesser extent regional emissions (section 3.4).

3.3. BC From Forest Fires

The dominant source of biofuel BC deposited at SCG is likely from regional forest fires; however, wood heating, agricultural burning, and land clearing are additional regional sources. Previous research in the Olympic Mountains in Washington State documented that BC emissions from forest fires resulted in rBC concentrations in snow in excess of 3,000 ng/g (Kaspari et al., 2015). BC deposition from a nearby forest fire on SCG was observed during extraction of the ice core in 1994 (supporting information), and many dark bands characteristic of forest fire deposition or melt consolidation (section 3.4) were observed throughout the record during processing. These visible layers have rBC concentrations two magnitudes greater than background levels (Table 1, Figure 2b).

The SCG rBC record is dissimilar to the forest fire emissions from the RCP database (Figures 2c and 2d), which is based on reconstructions of historical burned areas, and emission estimates based on vegetation maps (Mieville et al., 2010; Mouillot & Field, 2005). There are high uncertainties in the forest fire emissions inventory, with Mouillot and Field (2005) referring to them as a spatially explicit best guess. Large uncertainties include burnt area, allocation of burn surface to land cover type, biomass densities, burning efficiencies, and emission factors (Mieville et al., 2010). Thus, the dissimilarity between the records is not surprising.

Efforts to link high rBC horizons to individual forest fires for the period of overlap (1984–1991) using the Monitoring Trends in Burn Severity database were unsuccessful; however, consideration of the recurrence interval of fire in montane forests in Washington State indicates that BC emissions from forest fires could regularly result in BC deposition at SCG (supporting information). In summary, forest fires are a likely source of the observed anomalously high rBC horizons preserved in the record, consistent with Kaspari et al. (2015).

3.4. Melt Consolidation of BC

Another possible origin for the anomalously high rBC horizons is melt consolidation, during which multiple years of LAP deposition are concentrated into a single layer. This may occur when summer melt exceeds the total snow accumulation deposited over the previous winter, resulting in consolidation of 2 or more years of BC deposition. The 1953–1994 mass balance data provide insight into years where multiyear melt consolidation may have occurred. Mass balance at the core site was negative in 1979, which corresponds to elevated rBC concentrations (Figure S3). However, other years of negative mass balance (1988, 1989, and 1992–1994)

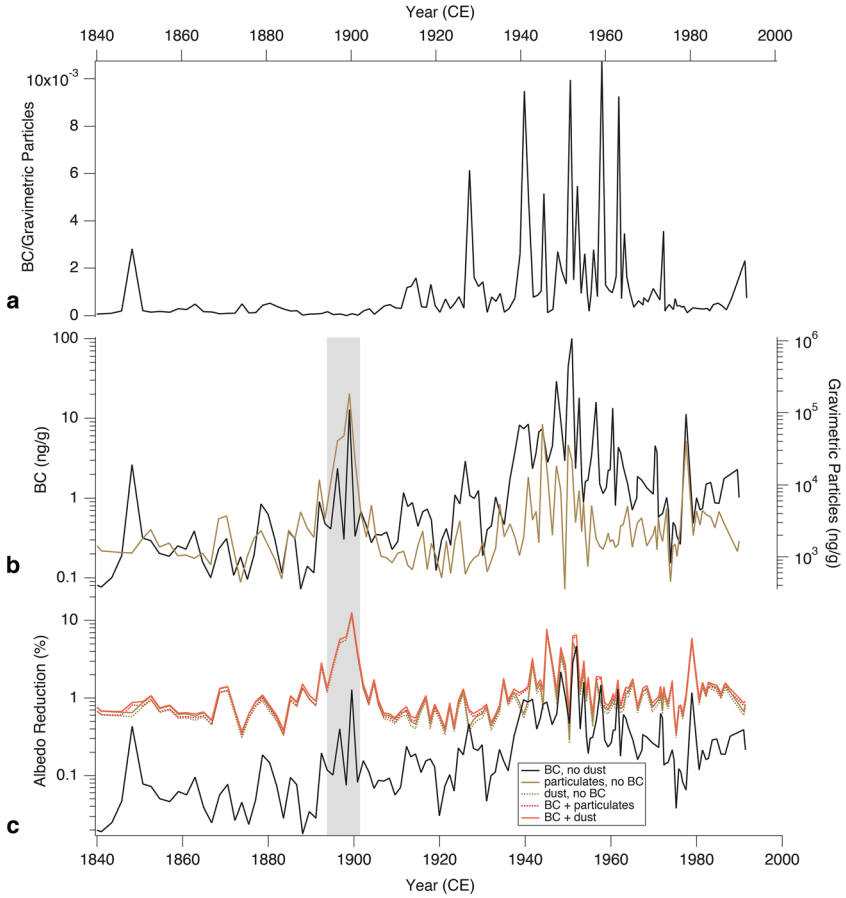

Figure 3. Year (CE) based on the highest probability dating scenario versus (a) black carbon/gravimetric particle ratio; (b) black carbon (black line) and gravimetric particle (brown line) concentrations; and (c) SNICAR modeled albedo reductions. Further details on the albedo model scenarios are provided in Table 3. The gray highlighted rectangles identify portions of the record that have high melt, and the light absorbing particles are likely the result of englacial flow rather than aeolian deposition.

do not correspond to notably elevated rBC concentrations, potentially due to low atmospheric BC loading or high enough melt to flush BC from the snowpack (Conway et al., 1996; Xu et al., 2012).

The BC/gravimetric particle ratio can be used to infer melt consolidation, assuming BC and dust are similarly affected by melt. The ratio of BC/gravimetric particles is elevated during the peak BC period spanning ~1940–1960, suggesting higher BC deposition during that period of time (Figure 3a). During 1977–1991, when BC concentrations again increase, the BC/gravimetric particle ratio is low, except for the most recent portion of the record in 1991. This suggests that melt consolidation plays a role in the post 1977 BC increasing trend, with higher BC deposition contributing to the elevated BC in 1991.

3.5. Comparison of SCG to Other Ice Core BC Records

The rBC time series from the SCG ice core differs from the other existing Northern Hemisphere rBC ice core records (Figure 4; the different dating scenarios minimally affect the presented results), with the timing of peak rBC concentrations at SCG later than in Greenland (McConnell et al., 2007; Sigl et al., 2018; Zdanowicz et al., 2018) and the European Alps (Sigl et al., 2018) and earlier than in the Caucasus (Lim et al., 2017), Himalayas (Kaspari et al., 2015), and Pamirs (M. Wang et al., 2015) (Figure 4). Greenland ice core records generally show BC concentrations increasing after 1880, peaking around 1910, followed by a decreasing trend during the latter 20th century, with North America interpreted as the dominant source of BC emissions deposited in Greenland. BC concentrations in the European Alps also begin to increase in the late 1800s but differ from Greenland in that BC concentrations remain elevated during much of the 20th century, with decreasing concentrations near the end of the 20th century. In contrast, rBC from the

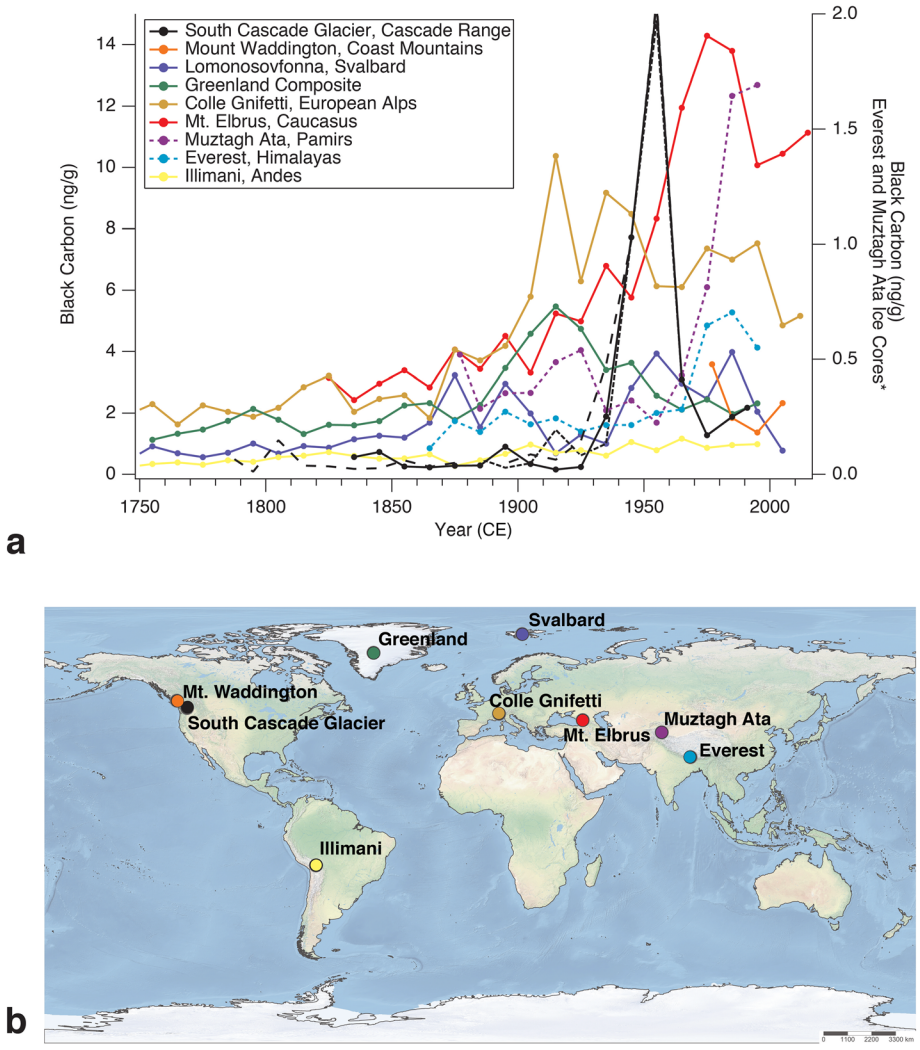

Figure 4. (a) Black carbon ice core records resampled to 10 year averages from South Cascade Glacier (this study based on the highest probability dating scenario; the dashed lines are based on the oldest and youngest dating scenarios); Mount Waddington, Coast Mountains (British Columbia; Neff et al., 2012); Lomnosovfonna, Svalbard (Arctic; Osmont et al., 2018); consolidated records from Greenland (Sigl et al., 2018); Colle Gnifetti, European Alps (Sigl et al., 2018); Mt. Elbrus, Caucuses (Lim et al., 2017); Muztagh Ata, Pamirs (Wang et al., 2015); Everest, Himalayas (Kaspari et al., 2011); and Illimani, Andes (Osmont et al., 2019). All records are plotted on the left *y*-axis, except for Muztagh Ata and Everest, which are plotted on the right *y*-axis. Samples from Everest and Muztagh Ata were stored as liquid, and the measured rBC concentrations underestimate actual BC concentrations. (b) Map showing the location of the BC ice core records.

SCG ice core increases slowly beginning around 1920, with peak concentrations between 1940–1960. rBC concentrations then decrease to the late 1970s, after which rBC concentrations again increase until the most recent part of the record.

The nearest ice core BC record to SCG is from Mount Waddington (51.3858°N, 125.2588°W; 3,000 m a.s.l.) in southwest British Columbia spanning 1973–2010 (P. Neff et al., 2012). For the limited period of overlap of the two records, the rBC concentrations are similar (Figure 3). While there is a similar pattern in the BC records (relatively high concentrations early on, followed by a decrease and subsequent increase), there is an offset in the timing between the two records, indicating potentially different sources depositing BC to the two sites. The shorter length of the Mount Waddington record prevents a comparison with SCG of 20th century BC trends.

These BC ice core records demonstrate regional differences in the timing of peak BC concentrations associated with regional differences in the timing of industrialization and technology transitions, consistent with Bond et al. (2007). However, the emission inventories represent large regions, within which BC emissions may be spatially and temporally variable, and there are uncertainties associated with the emission inventories (section 3.2). Thus, the ice core records are highly valuable for providing historic reconstructions of BC emissions and deposition, important for assessing the role of BC radiative forcing in the atmosphere, as well as the role of BC in snow and glacier darkening and melt.

A comparison of the averaged decadal ice core BC concentrations from all sites indicates that SCG has the highest BC concentration (rBC = 15.5 ng/g average spanning 1950–1960), with Mt. Elbrus having nearly as high BC concentrations during the 1970s and 1980s (Figure 4). SCG concentrations in the late 19th and early 20th centuries are lower than those in the Arctic, Caucasus, and European Alps, likely because of the later time of industrialization in the region near SCG. Differences in BC emissions as well as proximity to BC sources, elevation, and atmospheric transport pathways all contribute to the variations between records.

3.6. Gravimetric Particulate and Mineral Dust Record

Thermogravimetric analysis was used to constrain the mineral dust component of particles deposited on SCG. Based on the particle samples obtained from the 2014 SCG surface snow samples, nonorganics account for 83% ($n = 6$) of the total particle mass. This figure was applied to estimate the mineral dust contribution to the total particle load for the ice core record (Figure 2a), as insufficient sample size precluded conducting thermogravimetric analyses on the ice core samples. For the following discussion of the gravimetric particle (which includes the organic component) and mineral dust ice core records, we generically refer to the records as "dust" as the trends in the two time series are identical.

Generally, dust concentrations were below 10^4 ng/g, with elevated concentrations between the periods dated as 1978–1980, 1945–1954, 1896–1901, and prior to 1840 (Figure 2). The high dust concentrations between 1978–1980 and 1945–1954 are interpreted to represent increased aeolian deposition, whereas the elevated concentrations deeper in the core (below 115-m w.e.; Figure S2) are likely caused by melt/englacial flow (discussed further below).

Two factors that contribute to the higher dust loads during 1978–1980 include (1) deposition of ash from the 7 August 1980 Mt. St. Helens eruption (see section 2.3.8) and (2) 1979 was a negative mass balance year and melt consolidation would cause the 1978 and 1979 summer layers to coalesce into one (Figure S3). The higher dust deposition during 1945–1954 likely reflects increased dust emissions or arid conditions in the region. Examination of temperature and precipitation data from Diablo Dam spanning 1915 to present did not demonstrate a clear linkage between periods of drought and/or warmer temperatures and the SCG dust record. Uncertainties in the depth age scale were accounted for in this analysis by comparing the highest probability and youngest and oldest dating chronologies to the historical temperature and precipitation data.

The orientation and distribution of dust layers in the ice core between 83- and 87-m w.e. (dated to 1896–1901) and below 117-m w.e. suggest that aeolian deposition was not responsible for the high particle loading in these portions of the core (Figure S5). Dust identified elsewhere in the core demonstrated even particle size distributions and horizontal deposition patterns consistent with aeolian transport and deposition (Figure S5). Between 83- and 87-m w.e. and below 117-m w.e., large dust particles were detected (in some instances >500 μm), indicating deposition from nearby erosion rather than long-distance transport (Tegen et al., 2004). Additionally, in some instances, these layers were ~30° from horizontal. While glacier movement could have contributed to the angle of the layers, the particle size and appearance of the layers did not suggest aeolian deposition. One hypothesis for the high dust concentrations is melt and englacial flow, resulting in formation of high dust concentration layers. Sources for the dust could be headwall erosion of local exposed rock into an open bergschrund near the ice core drill site, enabling sediment transport deep into the glacier. This would be consistent with englacial transport (Fountain & Walder, 1998). The high dust concentrations in the bottommost portion of the core may originate from the glacier bed, which is why samples from these depths were not considered for ^{210}Pb dating.

Table 2
SNICAR Run Scenarios and Associated Albedo Reductions (%) for Aeolian Deposited Layers Based on rBC and Dust Concentrations That Were Resampled to 1-m Depth Resolution

Scenario name	BC	Dust definition	Minimum albedo reduction (%)	Median (average) albedo reduction (%)	Maximum albedo reduction (%) aeolian deposited
BC, no dust	BC	No dust	0.0	0.2 (0.3)	4.7
Particles, no BC	No BC	Dust concentration based on all measured particles	0.3	0.9 (1.3)	7.6
Dust, no BC	No BC	Particles * 0.83 = dust	0.3	0.8 (1.0)	6.9
BC + particles	BC	Dust concentration based on all measured particles	0.4	1.3 (1.3)	7.7
BC + dust	BC	Particles * 0.83 = dust	0.3	0.9 (1.2)	7.0

Note. The scenarios with "particles" classify all measured gravimetric particles as mineral dust, whereas the scenarios with "dust" assume that 83% of the particle load is mineral dust, as constrained by the thermogravimetric analysis.

3.7. Contribution of BC and Dust to Albedo Reductions

SNICAR was used to assess the contribution of BC and dust to albedo reductions (Flanner et al., 2007). To apply the SNICAR model to the SCG, ice core required the gravimetric particle and rBC records to be resampled to the same resolution; thus, the rBC record was resampled to the same resolution as the particles. SNICAR was run for five scenarios (Table 2), with the assumption that the measured concentrations reflect BC and particulate concentrations that resided on the snow surface in the past. Because the ice core stratigraphy suggests that some of the dust preserved in the ice core is not the result of aeolian deposition (and thus had not resided at the glacier surface), here we exclude the portions of the core spanning 83- to 87-m w.e. and below 117-m w.e., as discussed in section 3.6. Particles/dust dominated albedo reductions the majority of the time (122 out of 129 samples). However, during the period of peak BC deposition (1940–1960), albedo reductions from BC and dust were comparable.

Because these albedo results (Table 2 and Figure 3) are coarsely resolved (based on 1-m depth resolution), they do not account for the actual particle concentrations that likely resided at the surface of the glacier. Thus, the SNICAR model was also run for scenarios based on the peak calculated dust and rBC surface concentrations (Figure S6). Eight samples were chosen based on visible particles deposited horizontally, consistent with surface deposition, rather than englacial flow (Table 3). The five rBC samples were chosen because they contained visually observable black layers and had high levels of detected rBC, while the three dust samples were chosen because they contained visually observable layers of yellow-brown particles and did not contain high levels of rBC. The thickness of the particle layers ranged from 2 to 4 mm in the eight samples. Based on the particle orientation, it was assumed that these layers previously resided at the surface of the glacier. To determine the hypothetic surface concentrations of the particle layers, the ice core sample length was divided by the observed particle layer thickness and multiplied by the measured concentration. To model calculated peak surface concentration for rBC (dust), the calculated surface rBC concentration and observed dust (rBC) concentration were used. For the clean snow, the rBC and dust concentrations were set to 0. The rBC and dust layer thicknesses ranged between 2–4 mm, which is thinner than the snow layer thickness that would affect snow albedo (S. McKENZIE Skiles & Painter, 2016). Thus, we also modeled albedo based on calculated rBC and dust surface concentrations assuming a 2-cm-thick layer.

The modeled albedo based on calculated peak rBC and dust concentrations is representative of late summer conditions when a season or more of particles would be concentrated at the surface and solar insolation is highest. For the layers with surface concentrations calculated based on the observed particle layer thickness, the rBC layers reduced broadband albedo by 42–53% relative to clean snow, while the dust scenarios reduced broadband albedo by 25–26% relative to clean snow (Tables 2 and 3; Figure S6). These results suggest that the largest albedo reductions based on the peak calculated concentrations were the result of BC deposition. These high concentration rBC layers most likely originated from regional forest fires. This is of concern,

Journal of Geophysical Research: Atmospheres

10.1029/2019JD031126

Table 3

SNICAR Run Scenarios and Associated Albedo Reductions (%) for Select High Concentration Layers Based on the Observed and 2-cm Particle Layer Thickness

Sample type	Depth (m)	Ice core sample length (m)	Observed particle layer thickness (m)	Sample observed rBC (ng/g)	Sample observed dust (ng/g)	Calculated surface concentration rBC based on observed particle layer thickness (ng/g)	Calculated surface concentration dust based on observed particle layer thickness (ng/g)	Calculated surface concentration rBC based on 2-cm-thick layer	Calculated surface concentration dust based on 2-cm-thick layer	Broadband albedo based on observed particle layer thickness	Broadband albedo based on 2-cm-thick layer
BC	49.51	0.08	0.002	459	32,000	18,400	-	1,836		0.32	0.61
BC	49.89	0.08	0.002	297	20,000	11,900	-	1,188		0.38	0.65
BC	50.18	0.09	0.002	277	19,000	12,500	-	1,247		0.37	0.64
BC	50.61	0.09	0.002	524	42,000	23,600	-	2,358		0.28	0.58
BC	53.75	0.07	0.002	309	31,000	10,800	-	1,082		0.39	0.66
Dust	11	0.17	0.004	0.6	141,000	-	6,000,000		1,198,500	0.55	0.59
Dust	50	0.39	0.004	2.8	42,000	-	4,100,000		819,000	0.56	0.61
Dust	86	1	0.003	0.5	81,000	-	27,000,000		4,050,000	0.55	0.56
Clean snow	-	-	-	-	-	-	-	-	-	0.81	0.81

Note. The scenarios with "particles" classify all measured gravimetric particles as mineral dust, whereas the scenarios with "dust" assume that 83% of the particle load is mineral dust, as constrained by the thermogravimetric analysis.

as drier, warmer conditions are projected to increase, resulting in an increase in the annual area burned by forest fires (Westerling et al., 2006; Wimberly & Liu, 2014). However, the results assuming that the BC and dust are distributed over a 2-cm-thick layer resulted in comparable albedo reductions, with BC and dust reducing broadband albedo by 15–23% and 20–25%, respectively. We thus conclude that dust dominated albedo reduction the majority of the time on SCG (Figure 3, Tables 2 and 3), with the exception of high concentration BC layers that likely originate from forest fires (Figure S6, Tables 2 and 3).

4. Conclusions

The SCG ice core provides the first ice core record of rBC deposition in the continental United States spanning ~1840–1991 and demonstrates that ice cores retrieved from temperate glaciers have the potential to provide valuable records of LAP deposition. Peak rBC deposition occurred between 1940–1960, when median rBC concentrations were 16 times higher than background, likely due to domestic coal and forest fire emissions (Table 1, Figure 2). SCG rBC concentrations decreased from 1960–1980, followed by an increasing trend to 1991 due to melt consolidation and an increase in regional emissions. Differences between the SCG record and BC emission inventories, as well as ice core records from other regions, indicate regional differences in the timing of anthropogenic and biomass BC emissions. The SCG record is thus a valuable contribution to understanding how BC emissions and deposition have varied spatially and temporally.

Isolated, low-frequency rBC concentrations up to two magnitudes higher than background levels were most likely the result of local forest fires and dry deposition of BC onto the glacial surface (Kaspari et al., 2015). While fire is a natural part of the ecosystem (Agee et al., 1990), forest fire activity in the United States has increased in frequency and intensity in recent decades due to earlier snowmelt (Westerling et al., 2006), as well as high fuel loads due to fire suppression activities (Clinton & Agee, 2004). Climate projections for the Pacific Northwest suggest that an increase in forest fires is likely as temperature rises and more winter precipitation falls as rain instead of snow, lowering fuel moisture levels in midsummer (Elsner et al., 2010; Wimberly & Liu, 2014). A consequence of larger and more frequent forest fires may be increased BC deposition on SCG, which would lower albedo and increase melt.

SCG dust deposition is variable throughout the record. High dust concentrations during 1978–1980 were linked to Mt. St. Helens ash deposition in 1980, as well as negative glacier mass balance during 1979 that likely caused the 1978 and 1979 layers to coalesce. High dust deposition during 1945–1954 may indicate arid conditions in the region. Based on the dust particle size distribution and exposed rock in the cirque surrounding the glacier, the dominant source of dust deposited on SCG likely originates from local sources. However, climate scenarios call for increased aridity in the Pacific Northwest, which may result in more dust generation locally and regionally (Elsner et al., 2010).

LAP albedo reductions on SCG are dominated by dust, with the exception of high concentration rBC layers that likely originate from forest fires and during the period of peak rBC concentrations during 1940–1960 when BC and dust similarly reduce albedo. The impact of LAP on albedo and melt is primarily during the dry summer months of June–October, when solar insolation is highest and the highest concentrations of LAP reside on the glacier surface due to dry deposition and melt consolidation. The presence of LAP can further lower albedo through the grain-size feedback, during which LAPs warm the snowpack and cause accelerated growth of snow grain size. This results in further albedo reductions, increasing the energy available for melt (S. M. Skiles et al., 2018). If the snow on the glacier is fully melted, bare glacier ice is exposed, which has a lower albedo than snow. This can result in upward migration of the snowline (Ryan et al., 2019). Thus, LAP can initiate a positive feedback and contribute to the observed negative glacier mass balance trend at SCG. On SCG during winter, heavy snow with low LAP concentrations is common (Delaney et al., 2015); thus, LAPs likely do not have a notable effect during the accumulation season.

The SCG ice core contributes to our knowledge of variations in historical BC emissions and deposition, which is important to understanding the role of BC in atmospheric radiative forcing. The SCG rBC and dust records also allowed the contributions of dust and BC to albedo reductions to be modeled and further understanding of the factors contributing to snow and glacier melt in the region. This is particularly important in Washington State, as snow and glaciers act as natural water reservoirs, providing agricultural and municipal water users a water supply during the dry summer months. Furthermore, melt water from glaciers in the

Cascades serves as a buffer during drought years when reduction in snowpack leads to reduced stream flow. Decreases in annual snowpack and glacial mass balance have been observed in the western United States since the 1950s (Mote et al., 2005; Pelto, 2008; Rasmussen, 2009), and this trend is projected to continue (Clarke et al., 2015; Elsner et al., 2010). With lower alpine snowpack, peak runoff occurs earlier in the year, leading to reduced stream flows in late summer when water is most needed (Elsner et al., 2010). Furthering our understanding of the factors contributing to historical snowmelt and glacier retreat has the potential to aid water managers in dealing with future water challenges.

Acknowledgments
This research was supported by a grant by the United States Geological Survey and State of Washington Water Research Center (2013WA372B). We thank Joan Fitzpatrick (USGS) and the drilling crew who collected the SCG ice core in 1994 and Matt Bachmann (USGS) for field support in 2014. Geoff Hargreaves and the National Ice Core Laboratory facilitated processing of the ice core. We thank Bob Jacobel for input on ash deposition from the 1980 Mt. St. Helens eruption, Andrew Fountain for input on basal flow velocities, and Jon Blundy, Wendy Bohrson, Angela Halfpenny, and Riley Blanchard for assistance in identification of the ash horizon in the SCG ice core. Mark Flanner (University of Michigan) created SNICAR lookup tables based on the range of observed impurity concentrations at SCG. Paul Winberry and Craig Scrivner assisted with SNICAR and RCP coding, respectively. Peter Neff provided the script used to run the Dansgaard-Johnsen model. Kazimierz Conder conducted the thermogravimetric analyses at the Paul Scherrer Institut. Angus Brookes created the location map. The BC and gravimetric impurity data are available at https://www.ncdc.noaa.gov/data-access/paleoclimatology-data/datasets/ice-core.

References

Agee, J. K., Finney, M., & Gouvenain, R. D. (1990). Forest fire history of Desolation Peak, Washington. *Canadian Journal of Forest Research*, *20*(3), 350–356. https://doi.org/10.1139/x90-051

Alexander, D. J., Davies, T. R. H., & Shulmeister, J. (2013). Basal melting beneath a fast-flowing temperate tidewater glacier. *Annals of Glaciology*, *54*(63), 265–271. https://www.cambridge.org/core/article/basal-melting-beneath-a-fastflowing-temperate-tidewater-glacier/325885A56B5A72B46363FEE409B9D062

Anslow, F., Hostetler, S., Bidlake, W., & Clark, P. (2008). Distributed energy balance modeling of South Cascade Glacier, Washington and assessment of model uncertainty. *Journal of Geophysical Research*, *113*, F02019. https://doi.org/10.1029/2007JF000850

Balkanski, Y., Schulz, M., Claquin, T., & Guibert, S. (2007). Reevaluation of mineral aerosol radiative forcings suggests a better agreement with satellite and AERONET data. *Atmospheric Chemistry and Physics*, *7*, 81–95. Article. <Go to ISI>://WOS:000243417800004

Bisiaux, M. M., Edwards, R., McConnell, J. R., Curran, M. A. J., Van Ommen, T. D., Smith, A. M., et al. (2012). Changes in black carbon deposition to Antarctica from two high-resolution ice core records, 1850–2000 AD. *Atmospheric Chemistry and Physics*, *12*(9), 4107–4115. Article. <Go to ISI>://WOS:000304055600017. https://doi.org/10.5194/acp-12-4107-2012

Bond, T., & Bergstrom, R. (2006). Light absorption by carbonaceous particles: An investigative review. *Aerosol Science and Technology*, *40*, 27–67.

Bond, T., Bhardwaj, E., Dong, R., Jogani, R., Jung, S., Roden, C., et al. (2007). Historical emissions of black and organic carbon aerosol from energy-related combustion, 1850–2000. *Global Biogeochemical Cycles*, *21*, GB2018. https://doi.org/10.1029/2006GB002840

Bond, T., Doherty, S., Fahey, D. W., Forster, P. M., Berntsen, T., DeAngelo, B. J., et al. (2013). Bounding the role of black carbon in the climate system: A scientific assessment. *Journal of Geophysical Research: Atmospheres*, *118*, 5380–5552. https://doi.org/10.1002/jgrd.50171

Buenning, N. H., Stott, L., Yoshimura, K., & Berkelhammer, M. (2012). The cause of the seasonal variation in the oxygen isotopic composition of precipitation along the western U.S. coast. *Journal of Geophysical Research*, *117*, D18114. https://doi.org/10.1029/2012JD018050

Clarke, G. K. C., Jarosch, A. H., Anslow, F. S., Radic, V., & Menounos, B. (2015). Projected deglaciation of western Canada in the twenty-first century. *Nature Geoscience*, *8*(5), 372–377. Article. <Go to ISI>://WOS:000353640100014

Clinton, S. W., & Agee, J. K. (2004). Fire and vegetation history in the Eastern Cascade Mountains, Washington. *Ecological Applications*, *14*(2), 443–459. http://www.jstor.org/stable/4493550

Conway, H., Gades, A., & Raymond, C. F. (1996). Albedo of dirty snow during conditions of melt. *Water Resources Research*, *32*, 1713–1718.

Dansgaard, W., & Johnsen, S. J. (1969). A flow model and a time scale for the ice core from Camp Century, Greenland. *Journal of Glaciology*, *8*(53), 215–223. https://www.cambridge.org/core/article/flow-model-and-a-time-scale-for-the-ice-core-from-camp-century-greenland/598BDE0C570955E3076C677CCC41B500

Delaney, I., Kaspari, S., & Jenkins, M. (2015). Black carbon concentrations in snow at Tronsen Meadow in Central Washington from 2012 to 2013: Temporal and spatial variations and the role of local forest fire activity. *Journal of Geophysical Research: Atmospheres*, *120*, 9160–9172. https://doi.org/10.1002/2015JD023762

Eichler, A., Schwikowski, M., Gaggeler, H. W., Furrer, V., Synal, H. A., Beer, J., et al. (2000). Glaciochemical dating of an ice core from upper Grenzgletscher (4200 m a.s.l.). *Journal of Glaciology*, *46*(154), 507–515. <Go to ISI>://WOS:000165920700017. https://doi.org/10.3189/172756500781833098

Elsner, M. M., Cuo, L., Voisin, N., Deems, J. S., Hamlet, A. F., Vano, J. A., et al. (2010). Implications of 21st century climate change for the hydrology of Washington State. *Climatic Change*, *102*(1-2), 225–260. ://WOS:000281978500010. http://link.springer.com/article/10.1007%2Fs10584-010-9855-0, https://doi.org/10.1007/s10584-010-9855-0

Flanner, M. G., Zender, C. S., Hess, P. G., Mahowald, N., Painter, T. H., Ramanathan, V., & Rasch, P. J. (2009). Springtime warming and reduced snow cover from carbonaceous particles. *Atmospheric Chemistry and Physics*, *9*, 2481–2497.

Flanner, M. G., Zender, C. S., Randerson, J. T., & Rasch, P. J. (2007). Present-day climate forcing and response from black carbon in snow. *Journal of Geophysical Research*, *112*, D11202. https://doi.org/10.1029/2006JD008003

Fountain, A. G., & Walder, J. S. (1998). Water flow through temperate glaciers. *Reviews of Geophysics*, *36*(3), 299–328. Review. <Go to ISI>://WOS:000076276300001

Gabrielli, P., Barbante, C., Bertagna, G., Bertó, M., Binder, D., Carton, A., et al. (2016). Age of the Mt. Ortles ice cores, the Tyrolean Iceman and glaciation of the highest summit of South Tyrol since the Northern Hemisphere Climatic Optimum. *The Cryosphere*, *10*(6), 2779–2797. https://www.the-cryosphere.net/10/2779/2016/, https://doi.org/10.5194/tc-10-2779-2016

Gäggeler, H. W., von Gunten, H., Rossler, E., Oeshger, H., & Schotterer, U. (1983). ^{210}Pb-dating of cold alpine firn/ice cores from Colle Gnifetti, Switzerland. *Journal of Glaciology*, *29*, 165–177.

Hadley, O. L., & Kirchstetter, T. W. (2012). Black-carbon reduction of snow albedo. *Nature Climate Change*, *2*, 437–440.

Hadley, O. L., Ramanathan, V., Carmichael, G. R., Tang, Y., Corrigan, C. E., Roberts, G. C., & Mauger, G. S. (2007). Trans-Pacific transport of black carbon and fine aerosols (D<2.5 um) into North America. *Journal of Geophysical Research*, *112*, D05309. https://doi.org/10.1029/2006JD007632

Hou, S., Jenk, T. M., Zhang, W., Wang, C., Wu, S., Wang, Y., et al. (2018). Age ranges of the Tibetan ice cores with emphasis on the Chongce ice cores, western Kunlun Mountains. *The Cryosphere*, *12*(7), 2341–2348. https://www.the-cryosphere.net/12/2341/2018/, https://doi.org/10.5194/tc-12-2341-2018

Hu, Z., Huang, J., Zhao, C., Ma, Y., Jin, Q., Qian, Y., et al. (2019). Trans-Pacific transport and evolution of aerosols: Spatiotemporal characteristics and source contributions. *Atmospheric Chemistry and Physics*, *19*(19), 12,709–12,730. https://www.atmos-chem-phys.net/19/12709/2019/, https://doi.org/10.5194/acp-19-12709-2019

IPCC (2013). *Climate change 2013: The physical science basis. Contribution of Working Group I to the Fifth Assessment Report of the Intergovernmental Panel on Climate Change*. United Kingdom and New York, NY, USA: Cambridge University Press.

Ito, A., & Penner, J. E. (2005). Historical emissions of carbonaceous aerosols from biomass and fossil fuel burning for the period 1870–2000. *Global Biogeochemical Cycles*, *19*, GB2028. https://doi.org/10.1029/2004GB002374

Jaffe, D., Anderson, T., Covert, D., Kotchenruther, R., Trost, B., Danielson, J., et al. (1999). Transport of Asian air pollution to North America. *Geophysical Research Letters*, *26*(6), 711–714. https://doi.org/10.1029/1999GL900100

Josberger, E. G., Bidlake, W. R., March, R. S., & Kennedy, B. W. (2017). Glacier mass-balance fluctuations in the Pacific Northwest and Alaska, USA. *Annals of Glaciology*, *46*, 291–296. https://www.cambridge.org/core/article/glacier-massbalance-fluctuations-in-the-pacific-northwest-and-alaska-usa/81BDFFA370D1E532441AA4DFB155EF02

Kaspari, S., Painter, T. H., Gysel, M., Skiles, S. M., & Schwikowski, M. (2014). Seasonal and elevational variations of black carbon and dust in snow and ice in the Solu-Khumbu, Nepal and estimated radiative forcings. *Atmospheric Chemistry and Physics*, *14*, 1–15.

Kaspari, S., Schwikowski, M., Gysel, M., Flanner, M. G., Kang, S., Hou, S., & Mayewski, P. A. (2011). Recent increase in black carbon concentrations from a Mt. Everest ice core spanning 1860–2000 AD. *Geophysical Research Letters*, *38*, L04703. https://doi.org/10.1029/2010GL046096

Kaspari, S., Skiles, S. M., Delaney, I., Dixon, D., & Painter, T. (2015). Accelerated glacier melt on Snow Dome, Mt. Olympus, Washington, USA, due to deposition of black carbon and mineral dust from wildfire. *Journal of Geophysical Research: Atmospheres*, *120*, 2793–2807. https://doi.org/10.1002/2014JD022676

Lim, S., Fain, X., Ginot, P., Mikhalenko, V., Kutuzov, S., Paris, J. D., et al. (2017). Black carbon variability since preindustrial times in the eastern part of Europe reconstructed from Mt. Elbrus, Caucasus, ice cores. *Atmospheric Chemistry and Physics*, *17*(5), 3489–3505. <Go to ISI>://WOS:000397827900001. https://doi.org/10.5194/acp-17-3489-2017

McCabe, G. J., & Fountain, A. G. (2013). Glacier variability in the conterminous United States during the twentieth century. *Climatic Change*, *116*(3-4), 565–577. Article. <Go to ISI>://WOS:000313737100007. http://download.springer.com/static/pdf/940/art%253A10.1007%252Fs10584-012-0502-9.pdf?auth66=1417738342_0581d35e02eecde172821082da69dfb2&ext=.pdf

McCarty, L. (2003). Coal in the Puget Sound region. Retrieved from https://www.historylink.org/File/5158

McConnell, J., Edwards, R. L., Kok, G. L., Flanner, M. G., Zender, C. S., Saltzman, E. S., et al. (2007). 20th-century industrial black carbon emissions altered arctic climate forcing. *Science*, *317*(5843), 1381–1384. https://doi.org/10.1126/science.1144856

Menking, J. A. (2013). Black carbon measurements of snow and ice using the single particle soot photometer: Method development and an AD 1852–1999 record of atmospheric black carbon from a Mount Logan ice core Central Washington University

Mieville, A., Granier, C., Liousse, C., Guillaume, B., Mouillot, F., Lamarque, J. F., et al. (2010). Emissions of gases and particles from biomass burning during the 20th century using satellite data and an historical reconstruction. *Atmospheric Environment*, *44*(11), 1469–1477. http://www.sciencedirect.com/science/article/pii/S1352231010000373, https://doi.org/10.1016/j.atmosenv.2010.01.011

Miller, R. L., & Tegen, I. (1998). Climate response to soil dust aerosols. *Journal of Climate*, *11*, 3247–3267.

Ming, J., Cachier, H., Xiao, C., Qin, D., Kang, S., Hou, S., & Xu, J. (2008). Black carbon record based on a shallow Himalayan ice core and its climatic implications. *Atmospheric Chemistry and Physics*, *8*, 1343–1352.

Moosmuller, H., Chakrabarty, R. K., & Arnott, W. P. (2009). Aerosol light absorption and its measurement: A review. *Journal of Quantitative Spectroscopy & Radiative Transfer*, *110*(11), 844–878. Article; Proceedings Paper. <Go to ISI>://WOS:000267082200006

Morgenstern, U., & Taylor, C. (2009). Ultra low-level tritium measurement using electrolytic enrichment and LSC. *Isotopes in Environmental and Health Studies*, *45*(2), 96–117. http://www.tandfonline.com/doi/abs/10.1080/10256010902931194?url_ver=Z39.88-2003&rfr_id=ori:rid:crossref.org&rfr_dat=cr_pub%3dpubmed

Mote, P. W., Hamlet, A. F., Clark, M. P., & Lettenmaier, D. P. (2005). Declining mountain snowpack in western North America. *Bulletin of the American Meteorological Society*, *86*(1), 39. ://WOS:000226970100020–50. http://journals.ametsoc.org/doi/pdf/10.1175/BAMS-86-1-39

Mouillot, F., & Field, C. B. (2005). Fire history and the global carbon budget: A 1°× 1° fire history reconstruction for the 20th century. *Global Change Biology*, *11*(3), 398–420. https://doi.org/10.1111/j.1365-2486.2005.00920.x

Neff, J. C., Ballantyne, A. P., Farmer, G. L., Mahowald, N. M., Conroy, J. L., Landry, C. C., et al. (2008). Increasing eolian dust deposition in the western United States linked to human activity. *Nature Geoscience*, *1*(3), 189–195. Article. <Go to ISI>://WOS:000256433400019

Neff, P., Steig, E. J., Clark, D. H., McConnell, J., Pettit, E., & Menounos, B. (2012). Ice-core net snow accumulation and seasonal snow chemistry at a temperate-glacier site: Mount Waddington, southwest British Columbia, Canada. *Journal of Glaciology*, *58*. https://doi.org/10.3189/2012JoG3112J3078

Novakov, T., Ramanathan, V., Hansen, J. E., Kirchstetter, T. W., Sato, M., Sinton, J. E., & Sathaye, J. A. (2003). Large historical changes of fossil-fuel black carbon aerosols. *Geophysical Research Letters*, *30*(6), 1324. https://doi.org/10.1029/2002GL016345

Olivier, S., Blaser, C., Brütsch, S., Frolova, N., Gäggeler, H. W., Henderson, K. A., et al. (2006). Temporal variations of mineral dust, biogenic tracers, and anthropogenic species during the past two centuries from Belukha ice core, Siberian Altai. *Journal of Geophysical Research*, *111*, D05309. https://doi.org/10.1029/2005JD005830

McNeil, C. J., Sass, L. C., Florentine, C. E., Baker, E. H., Peitzsch, E. H., Whorton, E. N., et al. (2016). Glacier-wide mass balance and compiled data inputs: USGS benchmark glaciers, (ver. 4.0, November 2019). U.S. Geological Survey data release. https://doi.org/10.5066/F7HD7SRF

Osmont, D., Sigl, M., Eichler, A., Jenk, T. M., & Schwikowski, M. (2019). A Holocene black carbon ice-core record of biomass burning in the Amazon Basin from Illimani, Bolivia. *Climate of the Past*, *15*(2), 579–592. https://www.clim-past.net/15/579/2019/

Osmont, D., Wendl, I. A., Schmidely, L., Sigl, M., Vega, C. P., Isaksson, E., & Schwikowski, M. (2018). An 800-year high-resolution black carbon ice core record from Lomonosovfonna, Svalbard. *Atmospheric Chemistry and Physics*, *18*(17), 12,777–12,795. https://www.atmos-chem-phys.net/18/12777/2018/

Painter, T. H., Molotch, N., Cassidy, M. P., Flanner, M. G., & Steffen, K. (2007). Contact spectroscopy for the determination of stratigraphy of snow grain size. *Journal of Glaciology*, *53*, 121–127.

Pavlova, P. A., Jenk, T. M., Schmid, P., Bogdal, C., Steinlin, C., & Schwikowski, M. (2015). Polychlorinated biphenyls in a temperate alpine glacier: 1. Effect of percolating meltwater on their distribution in glacier ice. *Environmental Science & Technology*, *49*(24), 14,085–14,091. https://doi.org/10.1021/acs.est.5b03303

Pelto, M. S. (2008). Impact of climate change on north cascade alpine glaciers, and alpine runoff. *Northwest Science*, *82*(1), 65–75. Article. <Go to ISI>://WOS:000253880300006

Petzold, A., Ogren, J. A., Fiebig, M., Laj, P., Li, S. M., Baltensperger, U., et al. (2013). Recommendations for reporting "black carbon" measurements. *Atmospheric Chemistry and Physics*, *13*(16), 8365–8379. https://www.atmos-chem-phys.net/13/8365/2013/, https://doi.org/10.5194/acp-13-8365-2013

Ramanathan, V., & Carmichael, G. R. (2008). Global and regional climate changes due to black carbon. *Nature Geoscience*, *1*, 221–227.

Rasmussen, L. A. (2009). South Cascade Glacier mass balance, 1935–2006. *Annals of Glaciology*, *50*(50), 215–220. Article. <Go to ISI>://WOS:000279990100031

Rasmussen, L. A., Conway, H., & Hayes, P. S. (2000). The accumulation regime of Blue Glacier, USA, 1914–96. *Journal of Glaciology*, *46*(153), 326–334. <Go to ISI>://WOS:000090153900016

Riedel, J., & Larrabee, M. A. (2011). North Cascades National Park Complex glacier mass balance monitoring annual report, water year 2009: North Coast and Cascades Network. Retrieved from Fort Collins:

Ryan, J. C., Smith, L. C., van As, D., Cooley, S. W., Cooper, M. G., Pitcher, L. H., & Hubbard, A. (2019). Greenland ice sheet surface melt amplified by snowline migration and bare ice exposure. *Science Advances*, *5*(3), eaav3738. http://advances.sciencemag.org/content/5/3/eaav3738.abstract

Schultz, M. G., Heil, A., Hoelzemann, J. J., Spessa, A., Thonicke, K., Goldammer, J. G., et al. (2008). Global wildland fire emissions from 1960 to 2000. *Global Biogeochemical Cycles*, *22*, GB2002. https://doi.org/10.1029/2007GB003031

Schwantes, C. A. (1996). *The Pacific Northwest: An interpretive history*. Lincoln and London: University of Nebraska Press.

Schwarz, J. P., Doherty, S., Li, F., Ruggiero, S. T., Tanner, C. E., Perring, A. E., et al. (2012). Assessing recent measurement techniques for quantifying black carbon concentration in snow. *Atmospheric Measurement Techniques Discussions*, *5*(3), 3771–3795. https://doi.org/10.5194/amtd-5-3771-2012

Schwarz, J. P., Gao, R. S., Fahey, D. W., Thomson, D. S., Watts, L. A., Wilson, J. C., et al. (2006). Single-particle measurements of midlatitude black carbon and light-scattering aerosols from the boundary layer to the lower stratosphere. *Journal of Geophysical Research*, *111*, D16207. https://doi.org/10.1029/2006JD007076

Sigl, M., Abram, N. J., Gabrieli, J., Jenk, T. M., Osmont, D., & Schwikowski, M. (2018). 19th century glacier retreat in the Alps preceded the emergence of industrial black carbon deposition on high-alpine glaciers. *The Cryosphere*, *12*(10), 3311–3331. Article. <Go to ISI>://WOS:000447610400002

Skiles, S. M., Flanner, M., Cook, J. M., Dumont, M., & Painter, T. H. (2018). Radiative forcing by light-absorbing particles in snow. *Nature Climate Change*, *8*(11), 965. <Go to ISI>://WOS:000448839600015

Skiles, S. M., & Painter, T. (2016). Daily evolution in dust and black carbon content, snow grain size, and snow albedo during snowmelt, Rocky Mountains, Colorado. *Journal of Glaciology*, *63*(237), 118–132. https://www.cambridge.org/core/article/daily-evolution-in-dust-and-black-carbon-content-snow-grain-size-and-snow-albedo-during-snowmelt-rocky-mountains-colorado/9CF5A82C27E7994E2FA7333A121F1A69

Skiles, S. M., Painter, T., Deems, J., Bryant, A., & Landry, C. (2012). Dust radiative forcing in snow of the Upper Colorado River Basin: 2. Interannual variability in radiative forcing and snowmelt rates. *Water Resources Research*, *48*, W07522. https://doi.org/10.1029/2012WR011986

Sperazza, M., Moore, J. N., & Hendrix, M. S. (2004). High-resolution particle size analysis of naturally occurring very fine-grained sediment through laser diffractometry. *Journal of Sedimentary Research*, *74*(5), 736–743.

Tegen, I., Werner, M., Harrison, S. P., & Kohfeld, K. E. (2004). Relative importance of climate and land use in determining present and future global soil dust emission. *Geophysical Research Letters*, *31*, L05105. https://doi.org/10.1029/2003GL019216

Waitt Jr, R. B., & Dzurisin, D. (1981). Proximal air-fall deposits from the May 18 eruption (of Mount St. Helens)—Stratigraphy and field sedimentology (Vol. 1250).

Wang, C., Hou, S., Pang, H., Liu, Y., Gäggeler, H. W., Tobler, L., et al. (2014). ^{210}Pb dating of the Miaoergou ice core from the eastern Tien Shan, China. *Annals of Glaciology*, *55*(66), 105–110. https://www.cambridge.org/core/article/210-pb-dating-of-the-miaoergou-ice-core-from-the-eastern-tien-shan-china/FBAA5163FD58E486D93ABCE1E8925CF1, https://doi.org/10.3189/2014AoG66A151

Wang, M., Xu, B., Kaspari, S., Gleixner, G., Schwab, V., Zhao, H., et al. (2015). Century-long record of black carbon in an ice core from the Eastern Pamirs: Estimated contributions from biomass burning. *Atmospheric Environment*, *115*, 79–88. https://doi.org/10.1016/j.atmosenv.2015.05.034

Warren, S. (1984). Impurities in snow: Effects on albedo and snowmelt (review). *Annals of Glaciology*, *5*, 177–179.

Wendl, I., Menking, J. A., Farber, R., Gysel, M., Kaspari, S., Laborde, M., & Schwikowski, M. (2014). Optimized method for black carbon analysis in ice and snow using the single particle soot photometer. *Atmospheric Measurement Techniques*, *7*(8), 2667–2681. https://doi.org/10.5194/amt-7-2667-2014

Westerling, A. L., Hidalgo, H. G., Cayan, D. R., & Swetnam, T. W. (2006). Warming and earlier spring increase western US forest wildfire activity. *Science*, *313*(5789), 940–943. <Go to ISI>://WOS:000239817000035. http://www.sciencemag.org/content/313/5789/940.full.pdf

Wimberly, M. C., & Liu, Z. H. (2014). Interactions of climate, fire, and management in future forests of the Pacific Northwest. *Forest Ecology and Management*, *327*, 270–279. Article. <Go to ISI>://WOS:000340852800029

Xu, B., Cao, J., Joswiak, D., Liu, X., Zhao, H., & He, J. (2012). Post-depositional enrichment of black soot in snow-pack and accelerated melting of Tibetan glaciers. *Environmental Research Letters*, *7*(1), 014022. https://doi.org/10.1088/1748-9326/7/1/014022

Zdanowicz, C. M., Proemse, B. C., Edwards, R., Wang, F. T., Hogan, C. M., Kinnard, C., & Fisher, D. (2018). Historical black carbon deposition in the Canadian High Arctic: A > 250-year long ice-core record from Devon Island. *Atmospheric Chemistry and Physics*, *18*(16), 12,345–12,361. <Go to ISI>://WOS:000442775100002